Localized defect modes in finite metallic two-dimensional photonic crystals

T. Ochiai and J. Sánchez-Dehesa
Departamento de Física Teórica de la Materia Condensada, Facultad de Ciencias (C-5), Universidad Autónoma de Madrid, Madrid 28049, Spain

(Received 7 February 2002; published 12 June 2002)

We present a comprehensive analysis of localized defect modes in finite photonic crystals with an isolated defect by means of the multiple-scattering theory. The scattering cross section of such systems can show resonance peaks owing to the tunneling through the defect, from which the eigenfrequency, eigenfunction, irreducible representation, and quality factor of the corresponding defect modes are obtained. The method, which is first applied to two-dimensional photonic crystals composed of dielectric cylinders, shows a fairly good agreement with known results obtained by the other methods. The method is also applied to clusters consisting of Drude-type metallic cylinders in a square configuration, where the eigenfrequencies of the localized modes are predicted as a function of the radius of the defect cylinder.

DOI: 10.1103/PhysRevB.65.245111 PACS number(s): 42.70.Qs, 42.25.Bs, 02.20.−a, 61.72.Ji

I. INTRODUCTION

A photonic crystal (PC) with artificial defects has many potential applications as an active or passive photonic device. It can be a frequency selector, a light-emitting diode, a low threshold laser, etc. Thus, much effort has been devoted to study localized defect modes relevant to these applications. The traditional approach to study localized defect modes is to use the supercell method, in which the Bloch boundary condition is applied to a large supercell where the defect is embedded and the corresponding Maxwell's equations are solved in the frequency[1] or time domain.[2] Alternatively, it is possible to impose an absorbing boundary condition[3] to the supercell in the finite-difference time-domain (FDTD) method.[4–6] Recently, multiple-scattering methods have been introduced to describe the photonic properties of finite two-dimensional[7–10] (2D) and three-dimensional[11] (3D) PCs. In this formalism the spherical or cylindrical harmonics centered at each scattering object are employed as the basis set of the radiation field and thus good accuracy in numerical calculation is obtained for PCs made of nonoverlapping spheres or cylinders. In addition, since the multiple-scattering formalism is a kind of ''on-shell'' method, we can treat the objects with frequency-dependent dielectric function in an equal footing as the objects with constant dielectric function.

Here, a comprehensive analysis of localized defect modes is performed by means of multiple-scattering theory for finite dielectric and metallic 2D PCs. Thus, in what follows we restrict ourselves to PCs consisting of cylinders with infinite height, radius r, and dielectric constant ϵ_r aligned periodically in an uniform background with dielectric constant ϵ_b. We further restrict our study to the optical responses to the light with a $\mathbf{k}$ vector contained in the plane perpendicular to the cylindrical axis (z axis). Therefore, the multiple-scattering formalism is much simplified, because the decoupling of the radiation field into TE (transverse electric) and TM (transverse magnetic) polarization occurs. Though we present results for 2D PCs, the method can be extended to 3D PCs in a parallel way.

In order to investigate localized defect modes we focus our interest to the far-field responses of the finite PCs with a defect component created at the center. In particular, the scattering cross section is our concern. Several authors studied defect modes by monitoring the near-field transmittance of the PC.[7,9] However, we think the definition of the transmittance in the near field is a little bit ambiguous, because it could be affected by various surface effects. Instead, the far field is preferable to monitor the response of the PC with a defect. In this case surface modes does not contribute to the cross section owing to their evanescent feature. Thus, optical modes in bulk can be extracted well. If the corresponding infinite photonic crystal has a photonic band gap and supports a localized defect mode in the gap, the scattering cross section shows peak in the spectrum of the cross section as a function of frequency, which reveals a resonance tunneling through the defect mode. In addition, at the resonance frequency the radiation field is highly localized in the defect region. With these ingredients it is possible to obtain properties of the localized defect modes, that is, their eigenfrequencies, eigenfunctions, irreducible representations, and their corresponding quality factor.

Here, two typical PC systems are studied to demonstrate the validity, efficiency, and wide applicability of the method. One is a triangular array of dielectric cylinders in air for the case of TM polarization. The other is a square array of Drude-type metallic cylinders under TE polarization. The first case is chosen as a benchmark for our method because this structure was previously studied by means of the FDTD method.[12] Therefore, its defect mode is known very accurately. On the contrary, in the second case even the band structure of the infinite system is not well known because the frequency dependence of the dielectric function forbids to apply simple plane-wave expansion and FDTD methods to this system. In addition, for the TE polarization, the eigenstates associated to surface-plasmon excitations, which appear in the band structure, are not well approximated by a superposition of plane waves. So far, to the best of our knowledge, only a few papers[13–16] have reported the TE band structure of metallic cylinders with a frequency-dependent dielectric function and none has studied the point defect mode in detail.

The paper is organized as follows. After giving a brief summary of the multiple-scattering theory, the method to extract properties of defect modes is explained in Sec. II. In Sec. III the method is applied to dielectric systems previously investigated by another method. In Sec. IV the method is applied to a Drude-type metallic system of cylinders without dissipation, where the eigenfrequencies of defect modes are calculated as a function of the defect size. Finally, Sec. IV summarizes the results.

II. OPTICAL RESPONSE OF FINITE PHOTONIC CRYSTALS

For clusters composed of infinitely long cylinders parallel to each other, there is a translational invariance along the z direction (the cylinders axis). This invariance allows the decoupling of the polarizations in the Maxwell equation, as far as the optical response within the plane perpendicular to the z direction is concerned. As a result, the vectorial Maxwell equation reduces to a pair of scalar equations:

$$\frac{1}{\epsilon(\mathbf{x})}\nabla^2\psi(\mathbf{x})+\frac{\omega^2}{c^2}\psi(\mathbf{x})=0 \quad \text{for TM}, \tag{1}$$

$$\nabla\cdot\left(\frac{1}{\epsilon(\mathbf{x})}\nabla\psi(\mathbf{x})\right)+\frac{\omega^2}{c^2}\psi(\mathbf{x})=0 \quad \text{for TE}. \tag{2}$$

Here, $\psi=H_z(E_z)$ for the TE (TM) polarization and a harmonic time dependence, which is specified by angular frequency ω, is assumed for the radiation field ψ. On the other hand, $\epsilon(\mathbf{x})$ denotes the position dependent dielectric function, where $\mathbf{x}$ is the 2D vector position $\mathbf{x}=(x,y)$.

In the multiple-scattering formalism the induced radiation field $\psi_\alpha^{\mathrm{ind}}(\mathbf{x})$ by the cylinder α centered at $\mathbf{x}_\alpha$ is expanded by the cylindrical harmonics around $\mathbf{x}=\mathbf{x}_\alpha$ as

$$\psi_\alpha^{\mathrm{ind}}(\mathbf{x})=\sum_l H_l(q_b|\mathbf{x}-\mathbf{x}_\alpha|)e^{il\theta(\mathbf{x}-\mathbf{x}_\alpha)}\psi_{\alpha,l}^{\mathrm{ind}}. \tag{3}$$

Here, l is the angular momentum, H_l is the Hankel function of first kind, $q_b\equiv\sqrt{\epsilon_b}\omega/c$, and $\theta(\mathbf{x})$ is the argument of $\mathbf{x}$. The multipole coefficient $\psi_{\alpha,l}^{\mathrm{ind}}$ is self-consistently determined by the following equation:[7–10]

$$\tilde{\psi}_\alpha^{\mathrm{ind}}=t_\alpha\left(\tilde{\psi}_\alpha^{\mathrm{ext}}+\sum_{\beta\neq\alpha}G_{\alpha\beta}\tilde{\psi}_\beta^{\mathrm{ind}}\right), \tag{4}$$

where $\tilde{\psi}_\alpha^{\mathrm{ind}}$ is a column vector whose lth component is $\psi_{\alpha,l}^{\mathrm{ind}}$. The first term in the parentheses of the above equation represents the incident external plane wave on the cylinder α, its explicit form being

$$(\tilde{\psi}_\alpha^{\mathrm{ext}})_l=i^l e^{i\mathbf{k}_i\cdot\mathbf{x}_\alpha-il\theta(\mathbf{k}_i)}, \tag{5}$$

where the plane wave has wave vector $\mathbf{k}_i(|\mathbf{k}_i|=q_b)$. The second term in the parentheses represents the contribution of the induced field by the other cylinders $\beta(\neq\alpha)$. Here $G_{\alpha\beta}$ is the propagator from β to α and is expressed by the Hankel function of first kind as

$$(G_{\alpha\beta})_{l,l'}=H_{l'-l}(q_b|\mathbf{x}_\alpha-\mathbf{x}_\beta|)e^{i(l'-l)\theta(\mathbf{x}_\alpha-\mathbf{x}_\beta)}. \tag{6}$$

The sum of these two terms can be regarded as the self-consistent incident wave for the cylinder α. The self-consistent scattered wave (induced field) by α is obtained by multiplying it with the t matrix, which is given by

$$(t_\alpha)_{l,l'}=\frac{-\epsilon_r\rho_b J_l(\rho_r)J_l'(\rho_b)+\epsilon_b\rho_r J_l(\rho_b)J_l'(\rho_r)}{\epsilon_r\rho_b J_l(\rho_r)H_l'(\rho_b)-\epsilon_b\rho_r J_l(\rho_b)H_l'(\rho_r)}\delta_{l,l'}, \tag{7}$$

for TE,

$$(t_\alpha)_{l,l'}=\frac{-\rho_b J_l(\rho_r)J_l'(\rho_b)+\rho_r J_l(\rho_b)J_l'(\rho_r)}{\rho_b J_l(\rho_r)H_l'(\rho_b)-\rho_r J_l(\rho_b)H_l'(\rho_r)}\delta_{l,l'} \tag{8}$$

for TM,

$$\rho_r=\frac{\omega}{c}\sqrt{\epsilon_r}r=q_r r, \quad \rho_b=q_b r. \tag{9}$$

The induced radiation field in the void between the cylinders is given as the sum of the induced fields by every α cylinder:

$$\psi^{\mathrm{ind}}(\mathbf{x})=\sum_\alpha \psi_\alpha^{\mathrm{ind}}(\mathbf{x}). \tag{10}$$

Inside the cylinder α the radiation field is given by

$$\psi_\alpha^{\mathrm{ins}}(\mathbf{x})=\sum_l J_l(q_r|\mathbf{x}-\mathbf{x}_\alpha|)e^{il\theta(\mathbf{x}-\mathbf{x}_\alpha)}(s_\alpha\tilde{\psi}_\alpha^{\mathrm{ind}})_l, \tag{11}$$

where s_α is an analog of the t matrix and relates the multiple components of the scattered field to those of the field inside the cylinder. Its expression is given by

$$(s_\alpha)_{l,l'}=-\frac{2i\epsilon_r}{\pi}\frac{1}{\epsilon_r\rho_b J_l(\rho_r)J_l'(\rho_b)-\epsilon_b\rho_r J_l(\rho_b)J_l'(\rho_r)}\delta_{l,l'} \tag{12}$$

for TE,

$$(s_\alpha)_{l,l'}=-\frac{2i}{\pi}\frac{1}{\rho_b J_l(\rho_r)J_l'(\rho_b)-\rho_r J_l(\rho_b)J_l'(\rho_r)}\delta_{l,l'} \tag{13}$$

for TM.

By truncating the angular momentum within $|l|\leqslant l_{\max}$, Eq. (4) reduces to a linear equation where the dimension of the relevant matrix is $N(2l_{\max}+1)$,N being the number of cylinders in the clusters. Thus, this equation can be numerically solved by Gaussian elimination.

An important physical quantity regarding the optical responses of the clusters is the scattering cross section of the cluster. The elastic differential cross section of the cluster is given by

$$\frac{d\sigma_{el}}{d\theta} = |f(\theta)|^2, \tag{14}$$

$$f(\theta) = \sum_{l,\alpha} \sqrt{\frac{2}{\pi q_b}} e^{-iq_b \hat{\mathbf{x}}\cdot\mathbf{x}_\alpha + il\theta}(-i)^{l+1}\psi^{\mathrm{ind}}_{\alpha,l}, \tag{15}$$

$$\hat{\mathbf{x}} = (\cos\theta, \sin\theta). \tag{16}$$

Finally, the total cross section including absorption is obtained with the optical theorem as

$$\sigma_{\mathrm{tot}} = 2\sqrt{\frac{2\pi}{q_b}}\mathrm{Im} f(\theta(\mathbf{k}_i)). \tag{17}$$

These quantities are relevant to the far-field distribution. In order to analyze the near-field response, the field configuration given by Eqs. (10) and (11) along with the electromagnetic energy inside the cylinders are needed.

Let us remark that Eq. (4) with vanishing $\tilde{\psi}^{\mathrm{ext}}_\alpha$ is the cluster version of the Korringa-Kohn-Rostoker (KKR) equation for 2D PCs.[17–19] In fact, the KKR equation is obtained from Eq. (4) by taking into account the Bloch theorem in the unit cell. From this point of view, in a large cluster we expect that the cluster version of the KKR determinant defined by

$$D_N(\omega) \equiv \det[\,\delta_{ll'}\delta_{\alpha\beta} - (t_\alpha G_{\alpha\beta})_{l,l'}(1-\delta_{\alpha\beta})] \tag{18}$$

has a zero in the complex plane of ω. The real part ω_c of the zero corresponds to an eigenfrequency of the infinite photonic crystal and the imaginary part $\Gamma/2$ of the zero is the resonance width. The width reduces as the cluster size increases and vanishes at infinite system. The ratio $Q \equiv \omega_c/\Gamma$ is identified as the quality factor of the resonance in the cluster. The zero causes a pole of $\psi^{\mathrm{ind}}_{\alpha,l}$ and σ_{tot} [through Eqs. (15) and (17)] in the complex plane of ω, and gives generally an asymmetric shape of the resonance as a function of frequency.

From the resonances we can extract properties of a localized defect mode as well as the eigenstates in a continuum spectrum. Normally, the resonance corresponding to an eigenstate in a continuum spectrum is broad for small clusters. However, the resonance corresponding to the defect mode in a band gap is quite sharp. Therefore, by looking for a sharp resonance in a band gap of the corresponding infinite photonic crystal, it is possible to identify the eigenfrequency of the defect mode. In addition, since the induced field is very concentrated in a defect region, effects of the external plane wave is negligible in this region. Thus, the localized defect mode can also be obtained by looking at the induced field ψ^{ind}.

If the PC with an isolated defect has a certain point-group symmetry, the defect mode can be classified according to the irreducible representations of that point group. In the case of the square and triangular lattices the relevant point groups are C_{4v} and C_{6v}, respectively. Let us suppose that the defect mode is attributed to an one-dimensional irreducible representation R. Under a point-group operation A the induced field at the resonance approximately satisfies

$$\psi^{\mathrm{ind}}(A^{-1}\mathbf{x}) = \chi_R(A)\psi^{\mathrm{ind}}(\mathbf{x}), \tag{19}$$

where $\chi_R(A)$ is the character of A in the representation R. In terms of the multipole coefficient the above equation can be written as

$$(\pm 1)^l \psi^{\mathrm{ind}}_{A^{-1}\alpha,\pm l} e^{\pm il\phi(A)} = \chi_R(A)\psi^{\mathrm{ind}}_{\alpha,l}, \tag{20}$$

where $\phi(A)$ is defined by

$$\theta(A^{-1}\mathbf{x}) = \pm\theta(\mathbf{x}) + \phi(A). \tag{21}$$

Since the irreducible representation can be identified by the characters of the point-group operations, we can extract the irreducible representation of the defect mode from Eq. (20) as follows.[20] Obviously, the numerical data of $\psi^{\mathrm{ind}}_{\alpha,l}$ for the truncated set of α,l approximately satisfies Eq. (20). Thus, from the data set, it is only possible to obtain the estimated value of the character $\chi^{\mathrm{est}}_R(A)$, which is the most plausible value of $\chi_R(A)$. By means of the least-squares method, the value is given by

$$\chi^{\mathrm{est}}_R(A) = \frac{\sum_{\alpha,l} \mathrm{Re}[(\pm 1)^l \psi^{\mathrm{ind}}_{A^{-1}\alpha,\pm l} e^{\pm il\phi(A)} (\psi^{\mathrm{ind}}_{\alpha,l})^*]}{\sum_{\alpha,l} |\psi^{\mathrm{ind}}_{\alpha,l}|^2}. \tag{22}$$

As will be seen in Sec. III, this value is very close to the true value of the character $\chi_R(A)$ in the representation R.

A few remarks concerning the symmetry characterization should be noted. Attention must be paid to the symmetry of the incident plane wave. If the plane wave is incident along a symmetric axis, e.g., the Γ-M direction of the triangular lattice, it cannot excite the resonance of the defect mode with odd parity with respect to the axis. This is because the incident plane wave is even with respect to the axis. Thus, by changing the angle of incidence we can selectively excite the defect modes. The second remark is concerning degenerate defect modes. If the defect mode is doubly degenerate, the induced field at the resonance can be well approximated as a linear combination of the eigenfunctions of the degenerate pair. For instance, the defect mode with the E representation of C_{4v} can be excited by the plane wave incident along any high-symmetry axis of the square lattice. This is because, the E mode always includes the component of the even parity with respect to the axis. On the other hand, the A_1 mode can also be excited by the plane wave along any high-symmetry axis. Thus, the E mode cannot be distinguished from the A_1 mode in this point of view. However, the possibility of the A_1 mode is excluded by looking at the field configuration along with the estimated value of the character at the resonance. The A_1 mode is symmetric with respect to any symmetry axis of the square lattice, whereas the E mode is not. As a result, the E mode can be distinguished from the A_1 mode.

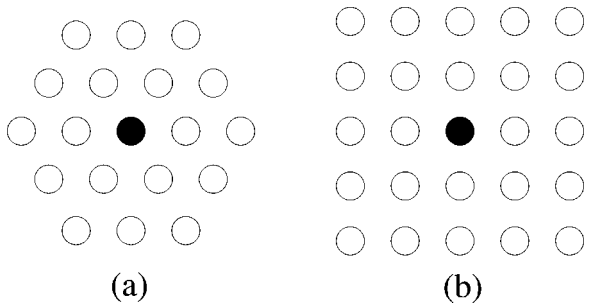

FIG. 1. Schematic illustration of the clusters used in numerical calculations. (a) n layers of cylinders arranged in a triangular lattice surrounding a defect cylinder. (b) n layers of cylinders arranged in a square lattice surrounding a defect cylinder. $n=2$ in both plots.

III. DIELECTRIC CYLINDERS AS A TEST EXAMPLE

In order to demonstrate how the method works, let us consider a cluster composed of a triangular array of dielectric cylinders as in Fig. 1(a). We assume $\epsilon_r=13, \epsilon_b=1$, and $r=0.2a$, where a is the lattice constant. As a defect, we simply remove the cylinder at the center of the cluster and n layers of the cylinders are assumed to be surrounding the defect cylinder [$n=2$ in Fig. 1(a)]. The band structure of the TM polarization of the corresponding infinite photonic crystal is shown in Fig. 2. There are two band gaps in the concerned frequency range and the lower one supports a localized defect mode with the A_1 representation of C_{6v} when one cylinder is removed. The eigenfrequency of the defect mode is about $\omega a/2\pi c=0.39$ according to the FDTD method.[12] As discussed before, the defect mode produces a peak in the scattering cross section of the cluster due to the resonant tunneling through the defect mode.

The comparison of the backwards differential cross sections of the clusters with and without the defect is shown in Fig. 3. A remarkable feature in the spectra is the appearance of a plateau at the photonic band-gap positions.[10] This comes from rigid reflection of the incident wave due to zero density of state in the band gaps. Besides, for the cluster with defect, we can see a dip around $\omega a/2\pi c=0.39$ in the plateau. This dip is caused by the resonant tunneling through the localized defect mode. The width of the dip is considerably narrow even at three surrounding layers. This also indicates the defect mode has very high Q. The radiation field at the frequency of the dip is highly localized in the defect and the A_1 symmetry of the defect mode can be seen clearly in Fig. 4. The numerical estimation of the characters by the least-squares method is listed in Table I. The values indicate that the localized defect mode is certainly attributed to A_1.

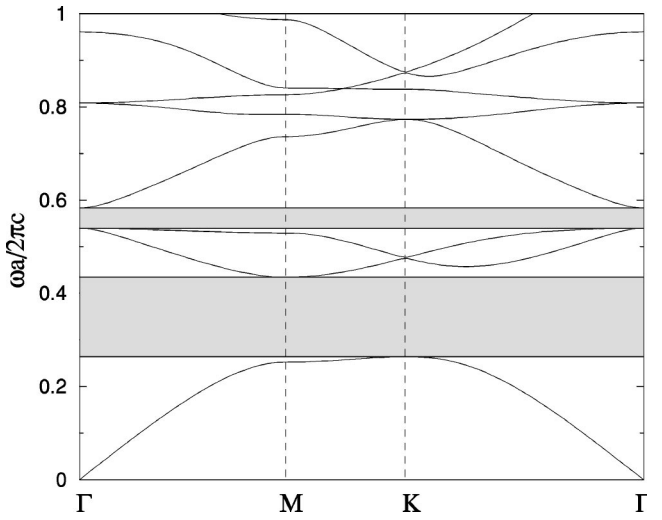

FIG. 2. Photonic band structure for the TM modes of the corresponding infinite photonic crystal shown in Fig. 1(a). The shaded regions define the band gaps. The following parameters were used: $\epsilon_r=13, \epsilon_b=1$, and $r=0.2a$.

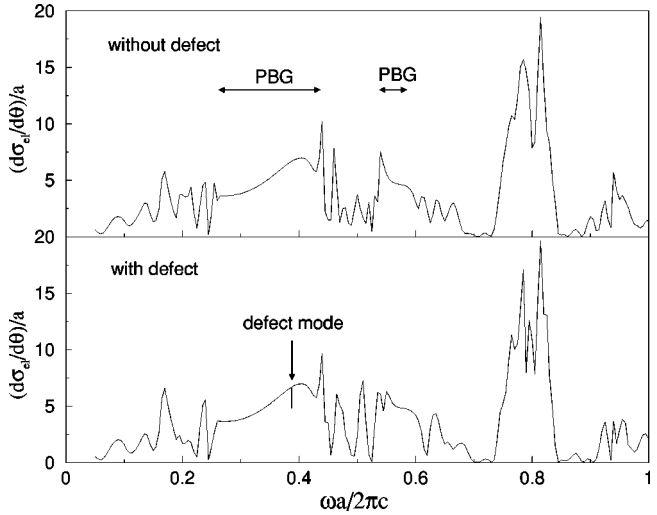

FIG. 3. Frequency dependence of the backwards differential cross section of two clusters with three surrounding layers. The upper(lower) panel shows the cluster without(with) a defect. The external plane wave impinges the cluster along the Γ-M direction [$\theta(\mathbf{k}_i)=30°$]. The material parameters are the same as in Fig. 2.

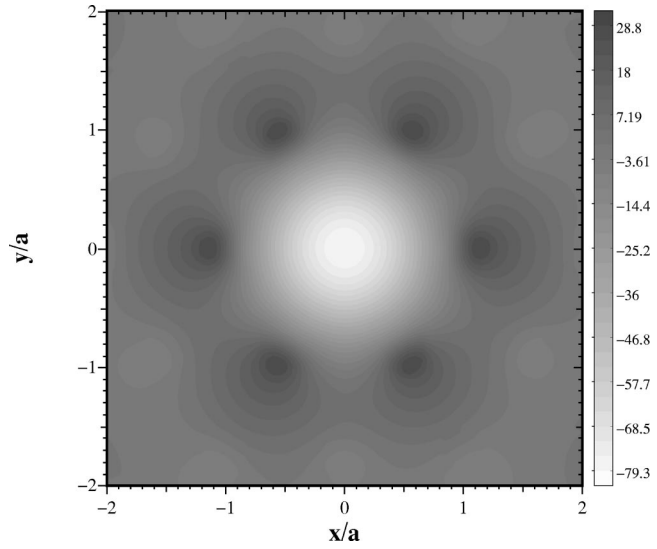

FIG. 4. The radiation field at the resonance frequency $\omega a/2\pi c=0.387\,89$ in the cluster with four surrounding layers. The external plane wave is incident along Γ-M[$\theta(\mathbf{k}_i)=30°$] of the triangular lattice.

TABLE I. Numerically estimated characters of C_{6v} for a localized defect mode in a hexagonal lattice. The values indicate that we can attributed a representation A_1 to the mode.

	$2C_6$	$2C_3$	C_2	$3\sigma_y$	$3\sigma_x$
χ_R^{est}	0.998 870	0.998 911	0.998 948	0.998 870	0.998 911

Let us have a close look at the resonance shape as a function of frequency. The left panel of Fig. 5 shows the cluster size dependence of the resonance shape in the total cross section. Notice that the resonance shape changes as the number of the surrounding layers increases, and it is generally asymmetric as was discussed before. The resonant frequency ω_c converges to a certain value that can be identified to the eigenfrequency of the localized defect mode in the infinite photonic crystal. On the other hand Γ reduces exponentially as N increases. As a consequence, the quality factor Q of the defect mode, which is shown in the right panel of Fig. 5, also increases with N. We can see that an extremely high Q value (larger than 10 000) is achieved with four surrounding layers. Nevertheless, let us point out the exponentially growing Q factor is generally prohibited in real material. In fact, the positive imaginary part in the dielectric constant is not negligible in real material. This causes a dielectric loss that generally makes the Q factor saturated as N increases.[21,22]

IV. METALLIC CYLINDERS

Next, let us consider a cluster composed of a square array of metallic cylinders as Fig. 1(b). As mentioned before, the multiple-scattering formalism is a kind of ''on-shell'' method, so that it can treat metallic components with frequency-dependent dielectric constant. For simplicity, we assume the cylinders of the Drude metal whose dielectric constant is given by

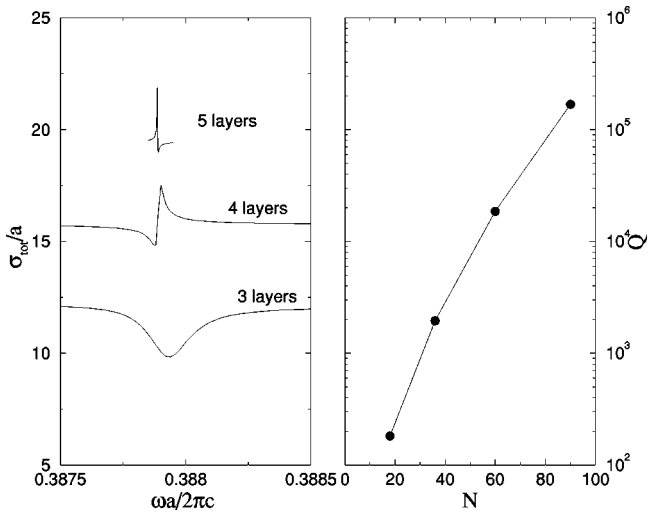

FIG. 5. (Left panel) Behavior of the resonance shape in the total cross section as a function of the surrounding layers. Note that the width of the panel is 0.001 in normalized units of frequency. (Right panel) Quality factor of the resonance Q plotted as a function of the number N of cylinders in the cluster.

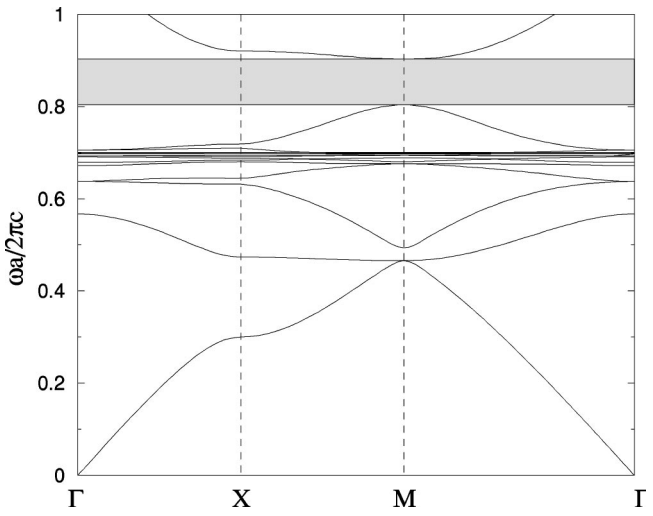

FIG. 6. The photonic band structure of an square array of metallic cylinders. See text for the parameters used in the numerical calculation.

$$\epsilon_r(\omega)=\epsilon_\infty\left(1-\frac{\omega_p^2}{\omega^2}\right) \tag{23}$$

with $\epsilon_\infty=1.0$ and $\omega_p a/(2\pi c)=1.0$. The radius r of the cylinders is taken to be $0.3a$, where a is the lattice constant of the square lattice.

The TE band structure of the corresponding infinite PC is shown in Fig. 6. Here, we used the KKR method to calculate the photonic band structure. The angular momentum cutoff $l_{\max}$ in the band calculation was taken to be 7.

As can be seen in the figure, several bands around $\omega a/(2\pi c)=0.7$, are flat owing to the localized nature of the surface plasmon.[16] The number of these flat bands increase as $l_{\max}$ increases. This is due to the Drude dielectric function

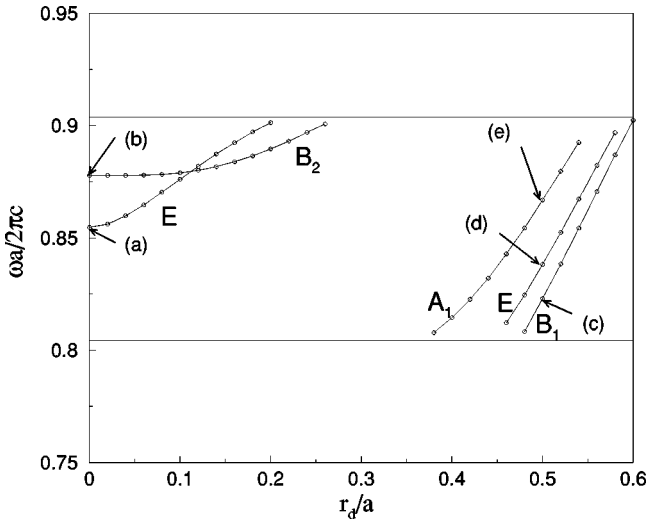

FIG. 7. Eigenfrequencies and their irreducible representations of localized defect modes in the photonic band gap of a square array of Drude-type metallic cylinders in air. The horizontal and vertical coordinate are the radius of the defect cylinder and the normalized frequency, respectively. See text for the parameters.

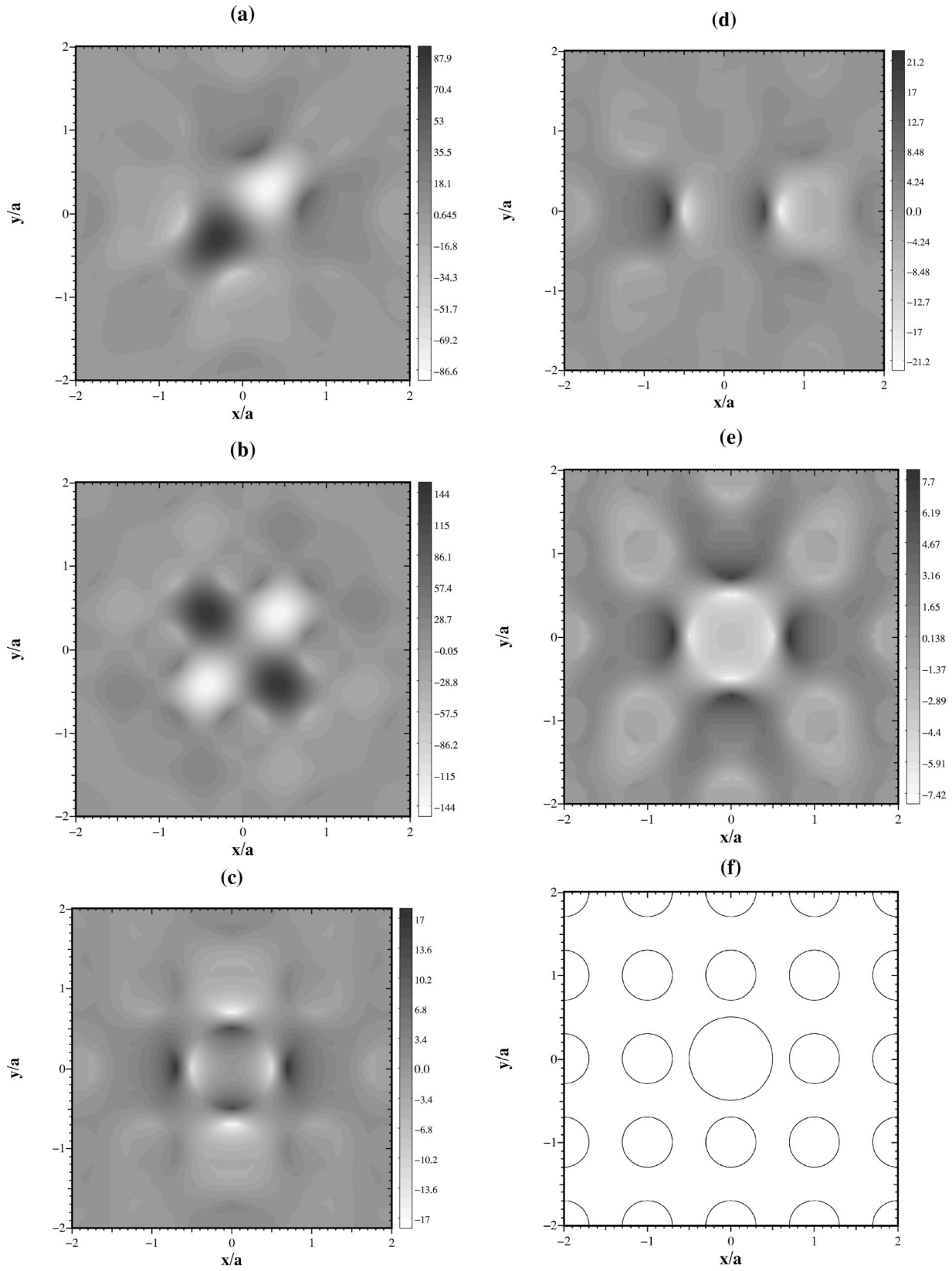

FIG. 8. Radiation fields at resonances corresponding to the (a), (b), (c), (d), and (e) points in Fig. 7 are shown in (a), (b), (c), (d), and (e), respectively. The resonance frequencies are $\omega a/2\pi c = 0.854\,75$ (a), 0.877 83 (b), 0.823 03 (c), 0.838 20 (d), and 0.866 87 (e). In (a) and (b) the external plane wave is incident along Γ-$M[\,\theta(\mathbf{k}_i) = 45°\,]$ of the square lattice and $r_d = 0$ was taken. In (c), (d), and (e) the external plane wave is incident along Γ-$X[\,\theta(\mathbf{k}_i) = 0°\,]$ and $r_d = 0.5a$. (f) shows the exact cluster used in the calculations for (c), (d), and (e).

Eq. (23). The cylinder with dielectric function Eq. (23) has a sequence of resonances, whose frequencies converge to the surface-plasmon frequency $\omega=\omega_p/\sqrt{2}$ as the angular momentum increases.[23] Thus, if we increase the cutoff from $l_{\max}$ to $l_{\max}+1$ in the band calculation, a new flat band appears. However, the eigenfrequencies of the rest of the bands are almost the same at both cutoffs $l_{\max}+1$ and $l_{\max}$, respectively, if $l_{\max}$ is large enough. In this sense a good convergence was achieved at $l_{\max}=7$ in the concerned frequency range.

A photonic band gap is obtained in $0.8043 \leqslant \omega a/2\pi c \leqslant 0.9038$. Thus, in this region we may expect that a localized defect mode appears when a structural defect is introduced. As a defect, we assume the cylinder of the Drude metal [Eq. (23)] with radius $r_d(\neq r)$. In this case the defect modes tend to avoid being localized in the defect cylinder, because the dielectric constant of the cylinders is negative in the gap. An interesting structure may be found if the defect cylinder touches the cylinders surrounding it. As was discussed by several authors,[24] the touching metallic cylinders causes a strong enhancement of the radiation field and a slightly different structure from separate cylinders is expected. In fact, we observed that near the touching condition $r_d=0.7a$ there is a very weak resonance that is difficult to identify in the spectrum of the cross section. This indicates that the defect mode corresponding to the resonance is not confined well in the cluster and that we must take larger clusters for characterization of the defect mode. The detailed investigation of this phenomenon is beyond the scope of the present paper. Thus, in the following we restrict ourselves to the range $0 \leqslant r_d \leqslant 0.6a$. By examining the optical responses of the defect clusters of Fig. 1(b), the eigenfrequency spectrum of the defect modes is determined. With regards to resonance shape, a behavior similar as Fig. 5 is observed, when the number of surrounding layers increases. In fact, three surrounding layers are enough to have a good convergence within four digits for the eigenfrequencies of the concerned defect modes.

Figure 7 shows the eigenfrequencies of the defect modes along with their irreducible representations as a function of r_d. The eigenfrequencies of the defect modes are increasing functions of the radius r_d, because $\delta\epsilon(\mathbf{x})$ is negative for positive δr_d.[25] As is seen in this figure, we have more than one defect mode at certain ranges of r_d. In addition a level crossing occurs between the B_2 and the E modes around $r_d=0.12a$.

The near-field images of the defect modes at the (a), (b), (c), (d), and (e) points in Fig. 7 are shown in Fig. 8. In Fig. 8(a) and 8(b) r_d is equal to zero and the external plane wave is incident along Γ-$M[\theta(\mathbf{k}_i)=45°]$ of the square lattice. In (a) the E mode is excited. As was discussed previously, only the mode with even symmetry among the degenerate pair of the E representation can be excited. The other mode of the degenerate pair can be excited by the plane wave with $\theta(\mathbf{k}_i)=-45°$. The field configuration is merely a replica of Fig. 8(a) rotated with 90°. As for (b), the B_2 symmetry of C_{4v} is clearly seen. In Figs. 8(c), 8(d), and 8(e) r_d is equal to $0.5a$ and the external plane wave is incident along Γ-$X[\theta(\mathbf{k}_i)=0°]$ of the square lattice. The localized nature of these defect modes, the B_1 symmetry for (c), and the A_1 symmetry for (e) are clearly seen in these figures. As for (d), the field configuration is of the even component with respect to the x axis among the degenerate pair of the E representation. Similarly as (a), the odd component is excited by the external plane wave with $\theta(\mathbf{k}_i)=90°$.

Compared to the resonances in Figs. 8(a) and 8(b), those in Figs. 8(c), 8(d), and 8(e) are weak in the average strength of the radiation field in the defect region and thus the radiation fields of (c), (d),and (e) are more extended than those of (a) and (b). This property is quite natural because the void between the cylinders, in which the radiation field is not evanescent in this case, becomes narrow for large r_d as it can be observed in Fig. 8(f).

V. SUMMARY

To conclude, this work has performed a comprehensive analysis of the localized defect modes in finite photonic crystals by the multiple-scattering theory. By using this theory, the eigenfrequency, the eigenfunction, the irreducible representation, and the quality factor of a localized defect mode can be predicted by looking at the sharp resonances in the scattering cross section. The method has been applied to two cases. First, a set of clusters consisting of a triangular array of dielectric cylinders have been studied and a good agreement concerning above properties with those by the FDTD method were obtained. Second, we have investigated a set of clusters composed of an square array of Drude-type metallic cylinders. In the latter case the eigenfrequency spectrum has been predicted as a function of the radius of the defect cylinder.

It should be emphasized that the method can be applied to 3D PCs made of dielectric or metallic spheres in a parallel way. In this case the dimension of the relevant equation is equal to $d \equiv 2N(l_{\max}+1)^2$. Thus, for large clusters the dimension is so large that much CPU time (proportional to d^3)is necessary for Gaussian elimination. Nevertheless, an efficient algorithm to solve the equation for 3D PCs was introduced recently.[11] By means of this algorithm, the CPU time needed is proportional to $N^2(l_{\max}+1)^3$, which is much smaller than d^3. Although the problem to find localized defect mode in 3D is much harder than that in 2D, we think that this approach can overcome the difficulties associated to the supercell method when it is applied to 3D PCs with a defect.

ACKNOWLEDGMENTS

The authors are grateful to F. J. García de Abajo for valuable discussions. This work was supported by the Project No. IST-1999-19009 PHOBOS of the European commission. We acknowledge the computing facilities provided by the Centro de Computación Científica at the Universidad Autónoma de Madrid.

[1] E. Yablonovitch, T.J. Gmitter, R.D. Meade, A.M. Rappe, K.D. Brommer, and J.D. Joannopoulos, Phys. Rev. Lett. **67**, 3380 (1991).
[2] K. Sakoda and H. Shiroma, Phys. Rev. B **56**, 4830 (1997).
[3] See, for example, A. Taflove, *Computational Electrodynamics* (Artech House, Boston, 1995).
[4] O. Painter, J. Vuckovic, and A. Scherer, J. Opt. Soc. Am. B **16**, 275 (1999).
[5] J-K. Hwang, H-Y. Ryu, and Y-H. Lee, Phys. Rev. B **60**, 4688 (1999).
[6] E. Miyai and K. Sakoda, Opt. Lett. **26**, 740 (2001).
[7] G. Tayeb and D. Maystre, J. Opt. Soc. Am. A **14**, 3323 (1997).
[8] L-M. Li and Z-Q. Zhang, Phys. Rev. B **58**, 9587 (1998).
[9] J. Yonekura, M. Ikeda, and T. Baba, J. Lightwave Technol. **17**, 1500 (1999).
[10] S. Nojima, Appl. Phys. Lett. **79**, 1959 (2001).
[11] F.J. García de Abajo, Phys. Rev. B **60**, 6086 (1999).
[12] K. Sakoda, J. Appl. Phys. **84**, 1210 (1998).
[13] V. Kuzmiak, A.A. Maradudin, and F. Pincemin, Phys. Rev. B **50**, 16 835 (1994).
[14] H. van der Lem and A. Moroz, J. Opt. A, Pure Appl. Opt. **2**, 395 (2000).
[15] X. Zhang, L-M. Li, Z-Q. Zhang, and C.T. Chan, Phys. Rev. B **63**, 125114 (2001).
[16] T. Ito and K. Sakoda, Phys. Rev. B **64**, 045117 (2001).
[17] K.M. Leung and Y. Qiu, Phys. Rev. B **48**, 7767 (1993).
[18] K. Ohtaka, T. Ueta, and K. Amemiya, Phys. Rev. B **57**, 2550 (1998).
[19] L.C. Botten, N.A. Nicorovici, R.C. McPhedran, C. Martijn de Sterke, and A.A. Asatryan, Phys. Rev. E **64**, 046603 (2001).
[20] T. Ochiai (unpublished).
[21] M.M. Sigalas, K.M. Ho, R. Biswas, and C.M. Soukoulis, Phys. Rev. B **57**, 3815 (1998).
[22] T. Ueta, K. Ohtaka, N. Kawai, and K. Sakoda, J. Appl. Phys. **84**, 6299 (1998).
[23] Exceptionally, the resonance of angular momentum $l=1$ is higher than those of $l \geqslant 2$ and makes the dominant contribution to form the highest band in eigenfrequency below the band gap.
[24] F.J. Garcia-Vidal and J.B. Pendry, Phys. Rev. Lett. **77**, 1163 (1996).
[25] J.D. Joannopoulos, R.D. Mead, and J.N. Winn, *Photonic Crystals* (Princeton University Press, Princeton, NJ, 1995), p. 72.